Current Biology 23, 58–63, January 7, 2013 ©2013 Elsevier Ltd All rights reserved http://dx.doi.org/10.1016/j.cub.2012.11.026

Report

Downregulation of the Mitochondrial Calcium Uniporter by Cancer-Related miR-25

Saverio Marchi,[1] Laura Lupini,[2] Simone Patergnani,[1] Alessandro Rimessi,[1] Sonia Missiroli,[1] Massimo Bonora,[1] Angela Bononi,[1] Fabio Corrà,[2] Carlotta Giorgi,[1] Elena De Marchi,[1] Federica Poletti,[1] Roberta Gafà,[3] Giovanni Lanza,[3] Massimo Negrini,[2] Rosario Rizzuto,[4] and Paolo Pinton[1,*]

[1]Section of General Pathology, Department of Morphology, Surgery and Experimental Medicine, Interdisciplinary Center for the Study of Inflammation (ICSI), Laboratory for Technologies of Advanced Therapies (LTTA)

[2]Department of Morphology, Surgery and Experimental Medicine

[3]Anatomic Pathology Section, Department of Morphology, Surgery and Experimental Medicine

University of Ferrara, 44121 Ferrara, Italy

[4]Department of Biomedical Sciences, University of Padua and CNR Neuroscience Institute, 35129 Padua, Italy

Summary

The recently discovered mitochondrial calcium uniporter (MCU) promotes Ca^{2+} accumulation into the mitochondrial matrix [1, 2]. We identified in silico miR-25 as a cancer-related MCU-targeting microRNA family and demonstrate that its overexpression in HeLa cells drastically reduces MCU levels and mitochondrial Ca^{2+} uptake, while leaving other mitochondrial parameters and cytosolic Ca^{2+} signals unaffected. In human colon cancers and cancer-derived cells, miR-25 is overexpressed and MCU accordingly silenced. miR-25-dependent reduction of mitochondrial Ca^{2+} uptake correlates with resistance to apoptotic challenges and can be reversed by anti-miR-25 overexpression. Overall, the data demonstrate that microRNA targeting of mitochondrial Ca^{2+} signaling favors cancer cell survival, thus providing mechanistic insight into the role of mitochondria in tumorigenesis and identifying a novel therapeutic target in neoplasia.

Results and Discussion

miR-25 Downregulates MCU and Protects from Ca^{2+}-Dependent Apoptosis

In the last two decades, mitochondrial Ca^{2+} homeostasis has been shown to participate in the control of the intrinsic pathway of apoptosis and to be influenced by oncogenes [3–6], thus suggesting that it is a signaling checkpoint in tumorigenesis. However, direct evidence and mechanistic insight were still lacking. The recent identification of the mitochondrial Ca^{2+} channel (mitochondrial calcium uniporter, MCU) [1, 2] and of the associated regulator MICU1 (also known as CBARA1) [7] now allow molecular investigation of the process, including the regulation of their expression by microRNAs (miRNAs). miRNAs are a class of small (19–25 nt), noncoding regulatory RNAs that regulate gene expression, causing target mRNA degradation or suppressing mRNA translation [8]. In human cancers, specific miRNAs are up- or downregulated, with consequent alteration in the expression of target proteins [9, 10].

By filtering the output of four target prediction algorithms (TargetScan [11], MicroT [12], MicroCosm [13], and miRanda [14]; see Table S1 available online), we identified five cancer-related miRNA families (miR-15, miR-17, miR-21, miR-25, and miR-137) that could be predicted to target MCU and/or MICU1. We thus tested their effect on mitochondrial Ca^{2+} homeostasis by expressing them in HeLa cells and measuring mitochondrial $[Ca^{2+}]$ with a targeted aequorin-based Ca^{2+} probe (mtAEQ) [15]. The data (Figure 1A) showed that only miR-25 caused a marked reduction in the $[Ca^{2+}]_m$ rise evoked by cell stimulation with 100 μM histamine, an agonist coupled to the generation of inositol 1,4,5-trisphosphate ($InsP_3$) and the release of Ca^{2+} from the endoplasmic reticulum (ER). Accordingly, overexpression of an anti-miR-25 increases the mitochondrial Ca^{2+} uptake to agonist stimulation (Figure S1A), with a slight decrease in cytosolic $[Ca^{2+}]$ ($[Ca^{2+}]_c$), probably due to increased Ca^{2+} clearance by mitochondria (Figure S1B).

The effects were predicted to depend on MCU downregulation. Indeed, the bioinformatics analysis of the 1,896 nt 3′ UTR of MCU revealed a 100% match target seed sequence for miR-25 at nt 1075–1081, highly conserved across seven species (Figure 1B), and insertion of the 759 nt 3′ UTR of MCU (but not of the 569 nt 3′ UTR of MICU1) downstream of the luciferase gene in a reporter plasmid led to significant miR-25-dependent decrease of reporter activity (Figures S1C and S1D). We thus tested MCU expression by immunoblotting and detected a marked reduction in the protein level upon miR-25 overexpression (Figure 1C) and an increase in anti-miR-25-expressing cells (Figure S1E). As expected, MCU mRNA abundance was significantly decreased by miR-25 (Figure 1D), whereas anti-miR-25 increased it (Figure S1F). MCU downregulation was also evident using an immunofluorescence technique: Figure S1G shows that miR-25 expression drastically decreased MCU antibody reactivity.

The effect of miR-25 is shared by the other members of the miRNA family: miR-92a and miR-363 target MCU mRNA and reduce MCU protein levels and, accordingly, inhibit mitochondrial Ca^{2+} uptake, without affecting $[Ca^{2+}]_c$ and $[Ca^{2+}]_{er}$ (data not shown).

We investigated whether miR-25-dependent reduction in mitochondrial Ca^{2+} uptake correlates with increased resistance to apoptotic challenges. Microscopy counts of cell viability after treatment with H_2O_2, C2-ceramide, or staurosporine (STS) revealed that miR-25-expressing HeLa cells were strongly protected from death caused by C2-ceramide and H_2O_2 (Figure 1E), apoptotic challenges for which mitochondrial Ca^{2+} loading acts as a sensitizing factor [16–18], whereas the sensitivity to STS was unaffected. Accordingly, PARP and caspase-3 cleavage upon C2-ceramide treatment were markedly reduced in miR-overexpressing cells (Figure 1F). These results were also confirmed by cellular positivity to the apoptotic marker annexin V (Figure S1H).

*Correspondence: paolo.pinton@unife.it

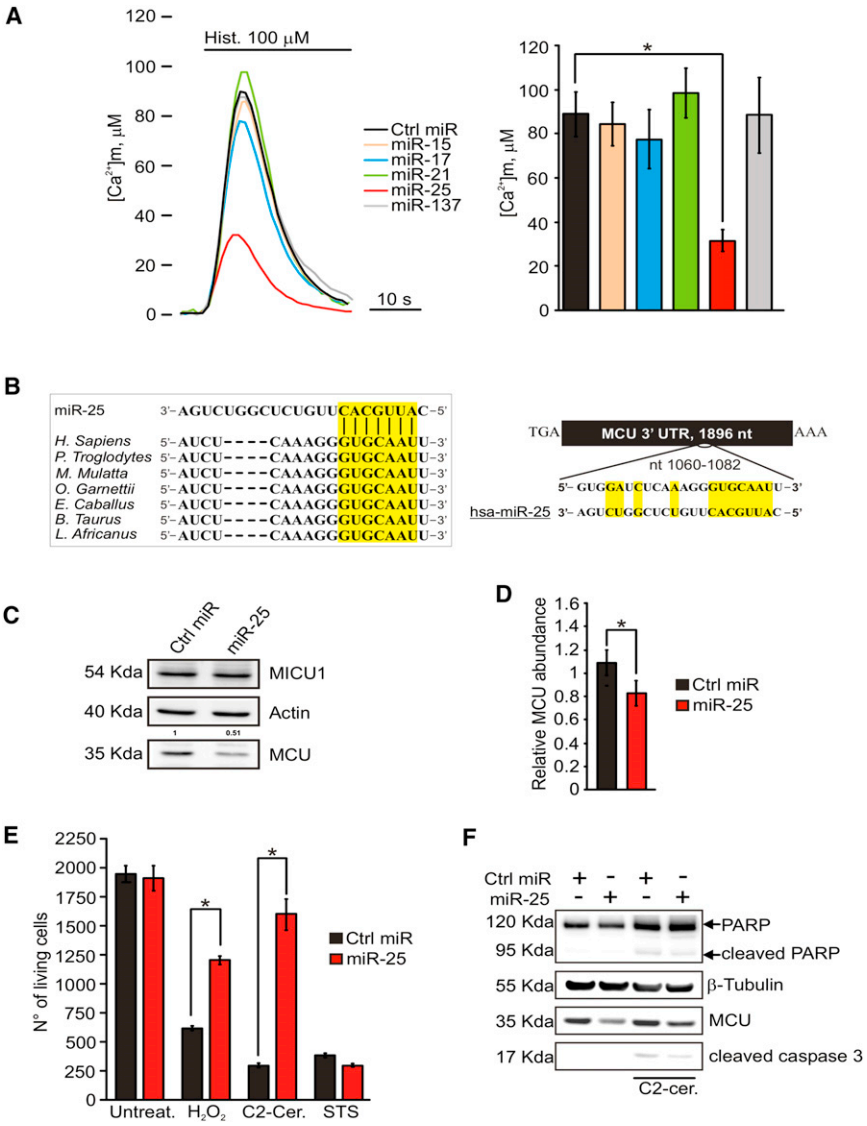

Figure 1. miR-25 Reduces $[Ca^{2+}]_m$ and Protects from Apoptosis by Downregulation of MCU mRNA and Protein Levels

(A) Mitochondrial and Ca^{2+} homeostasis in HeLa cells after expression of different miRNAs. Where indicated, mitochondrially targeted aequorin (mtAEQmut)-transfected cells were treated with 100 μM histamine (Hist.). Mitochondrial Ca^{2+} concentration ($[Ca^{2+}]_m$) peaks: negative control (Ctrl miR): 88.92 ± 10.05 μM; miR-15: 84.47 ± 9.96 μM; miR-17: 77.49 ± 13.23 μM; miR-21: 98.32 ± 11.09 μM; miR-25: 31.64 ± 5.06 μM; miR-137: 88.52 ± 17.12 μM. miR-25 induces an ~65% reduction of Ca^{2+} response. n = 18 independent experiments.

(B) The miR-25 seed sequence and its target in seven species; its target site resides at nt 1060–1082 of the MCU 3′ UTR. The middle seven nucleotides of miR-25 and its target region have been highlighted.

(C) Immunoblot for MCU and MICU1 after miR-25 expression in HeLa cells. Quantification of MCU protein is reported.

(D) MCU mRNA expression was assessed by quantitative real-time PCR in HeLa cells transfected with miR-25 or Ctrl miR. GAPDH expression was used to normalize MCU expression results for each sample. miR-25-enforced expression caused a 30% decrease in MCU mRNA levels, as compared to control transfected cells. n = 3 independent experiments.

(E) Microscopy counts of cell viability after treatment with hydrogen peroxide (H_2O_2; 500 μM for 2 hr) and C2-ceramide (C2-cer.; 40 μM for 2 hr) revealed that miR-25-expressing HeLa cells were protected from apoptosis, as compared to control (Ctrl miR). The number of living cells after staurosporine (STS; 10 μM for 1 hr) treatment appears unaffected by miR-25 expression. n = 3 independent experiments.

(F) Immunoblot shows reduced levels of cleaved PARP and cleaved caspase-3 in miR-25-expressing HeLa cells after treatment with C2-ceramide (C2-cer.; 40 μM for 2 hr).

See also Figure S1. In this and following figures, experiments are representative of more than three trials, and conditions are given in Experimental Procedures. *p < 0.05; error bars correspond to mean ± SEM.

miR-25 Induces Reduction of Mitochondrial Ca^{2+} Uptake Exclusively through MCU

We then proceeded to rule out that the effect on $[Ca^{2+}]_m$ was secondary to alterations of global Ca^{2+} signaling patterns or to morphological or functional dysregulation of mitochondria. On the former aspect, we investigated the cytosolic $[Ca^{2+}]$ changes and the state of filling and release kinetics of the ER. The results showed that miR-25, when expressed in HeLa cells, caused no difference in the amplitude of the $[Ca^{2+}]_c$ rise evoked by histamine (Figure 2A), nor in the steady state $[Ca^{2+}]_{er}$ or in the release caused by the agonist (Figure 2B). Thus, the effect of miR-25 on Ca^{2+} homeostasis is exclusively mitochondrial.

We then investigated the mitochondrial membrane potential ($\Delta\Psi m$), the driving force for Ca^{2+} accumulation, and the morphology of mitochondria, i.e., both the contacts with the ER (which were shown to be a critical determinant of rapid Ca^{2+} transfer between the two organelle [19–21]) and the formation of largely interconnected tubules, which favors Ca^{2+} diffusion within mitochondria. On the former aspect, measurements with the $\Delta\Psi m$-sensitive fluorescent dye tetramethylrhodamine methyl ester (TMRM) revealed no difference between miR-overexpressing and control HeLa cells (Figure 2C). As to morphology, mitochondrial labeling with the fluorescent probe mtDsRed showed that miR-25 overexpression causes no significant difference in mitochondrial volume or number (Figure 2D). Similarly, cotransfection with mtDsRed and an ER-targeted GFP showed no difference in the number of contact sites (Figure 2D, contact sites in white).

Overall, the data reveal that the $[Ca^{2+}]_m$ reduction caused by miR-25 should be ascribed to reduction of mitochondrial Ca^{2+} uptake through MCU. To further confirm this notion, we measured mitochondrial Ca^{2+} accumulation in permeabilized cells. For this purpose, HeLa cells were perfused with a solution mimicking the intracellular milieu (IB), supplemented with 2 mM EGTA, and permeabilized with digitonin for 1 min. The perfusion buffer was then changed to IB with an EGTA-buffered $[Ca^{2+}]$ of 4 μM (Figure 2E) or 1 μM (Figure 2F), eliciting a gradual rise in $[Ca^{2+}]_m$ that reached a plateau value of ~80 and ~20, respectively. At both buffered $[Ca^{2+}]$, miR-25

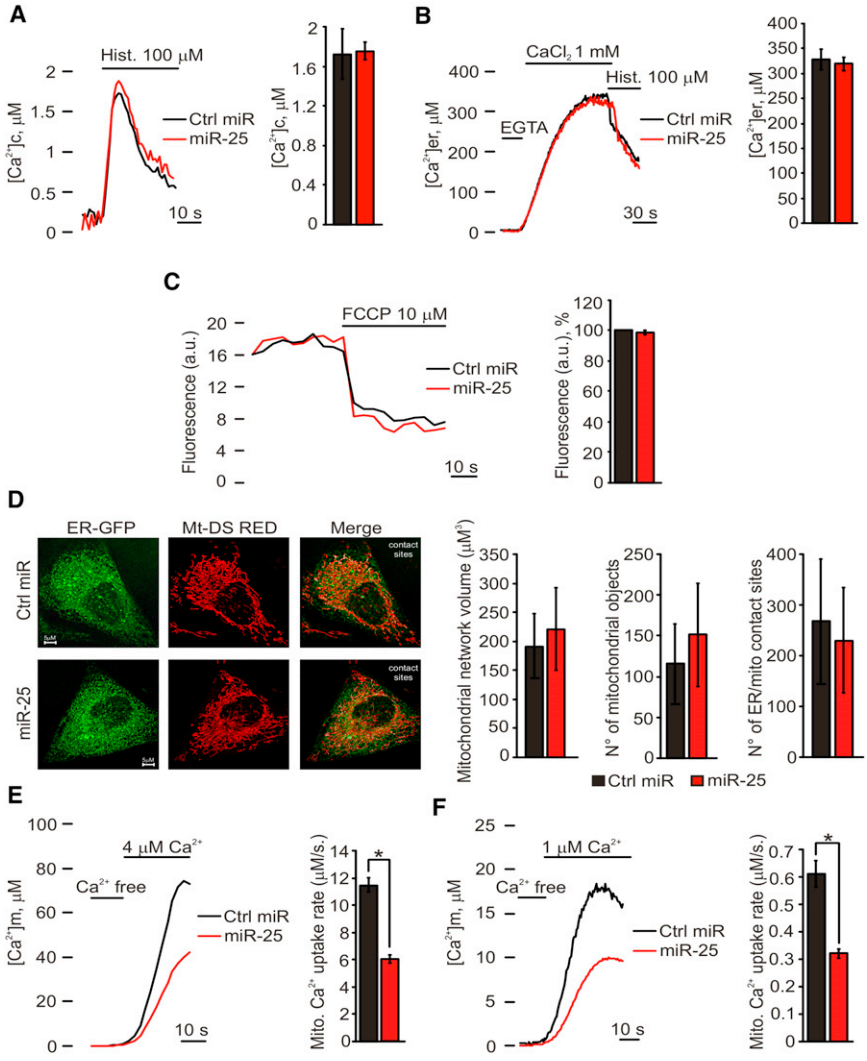

Figure 2. miR-25 Inhibits Mitochondrial Ca^{2+} Uptake without Causing Morphological Rearrangement or Changes in the Electrochemical Gradient

(A) Cytosolic Ca^{2+} concentration peaks: Ctrl miR: 1.72 ± 0.25 μM; miR-25: 1.726 ± 0.08 μM. n = 12 independent experiments.

(B) Reticular Ca^{2+} concentration levels: Ctrl miR: 328.2 ± 19.68 μM; miR-25: 319.4 ± 13.18 μM. n = 12 independent experiments.

(C) TMRM fluorescence measurements: miR-25-expressing HeLa cells show no difference in TMRM loading (−2.25 ± 1.18% compared to control cells). a.u., arbitrary units. n = 32 independent experiments.

(D) Fluorescence images of mtDsRed- and erGFP-labeled mitochondria and ER, respectively, in control- and miR-25-expressing HeLa cells. Mitochondrial volume and number were deduced by calculating object size (Ctrl miR: 191.49 ± 54.64 μm^3; miR-25: 221.16 ± 74.4 μm^3) and number (Ctrl miR: 115.56 ± 49 μm^3; miR-25: 151.67 ± 63.2 μm^3). ER/mitochondria colocalization was estimated by the average volume of overlapping areas (Ctrl miR: 267.89 ± 123.93 μm^3; miR-25: 230.7 ± 103.26 μm^3). n = 10 independent experiments.

(E and F) $[Ca^{2+}]_m$ in permeabilized cells stimulated with 4 μM (mitochondrial Ca^{2+} uptake rate: Ctrl miR: 11.44 ± 0.49 μM/s; miR-25: 6.01 ± 0.31 μM/s; E) or 1 μM (mitochondrial Ca^{2+} uptake rate: Ctrl miR: 0.61 ± 0.04 μM/s; miR-25: 0.32 ± 0.01 μM/s; F) EGTA-buffered fixed $[Ca^{2+}]$. n = 14 independent experiments.

*p < 0.05; error bars correspond to mean ± SEM. See also Figure S2.

overexpression causes a marked reduction in the rate of Ca^{2+} accumulation into mitochondria.

Mitochondrial Ca^{2+} alterations induced by miR-25 could be reverted by MCU re-expression in miR-25-expressing cells (Figure S2A) and, accordingly, this rescued Ca^{2+} affinity was mirrored in enhanced susceptibility to Ca^{2+}-dependent apoptosis (Figure S2B). Moreover, 22Rv1 prostatic cells, which possess very high levels of miR-25 (see Figure 3), were strongly sensitized to apoptosis after MCU overexpression (Figure S2C). The increased ability of mitochondria to accumulate Ca^{2+} is a fundamental aspect in MCU-related promotion of cell death: indeed, apoptosis induction observed in MCU-overexpressing HeLa cells was almost abolished in the presence of intracellular Ca^{2+} buffer BAPTA (Figure S2D).

Finally, although miR-25 has also been reported to exert antiapoptotic effects via interference with the expression of proapoptotic proteins, such as Bim [22], TRAIL [23], and PTEN [24], these results show how MCU can be considered a fundamental target of miR-25-dependent apoptosis inhibition.

Inhibition of MCU Levels by miR-25 Is a Key Aspect in Human Colon Cancer Progression

We then extended the analysis to cancer cells and tissues. We first evaluated cell lines derived from human carcinomas, in which miR-25 was reported to be highly expressed [24–26]. Both in PC3, LnCaP, and 22Rv1 (derived from prostate cancer) and in HCT116, RKO, SW80, and WiDr (derived from colon cancer) cell lines, we detected an inverse correlation between miR-25 levels and MCU mRNA expression, with high miR-25 levels and low MCU expression levels in cancer lines, compared to primary nonneoplastic cells (Figure 3A). We then directly investigated human poorly differentiated colonic adenocarcinoma samples by immunohistochemistry and microarray. Also in this case, a significant difference in miR-25 expression levels was detected (Figure 3B), which correlates with a downregulation of MCU expression. Indeed, in colonic adenocarcinoma samples with high miR-25 expression levels, MCU was virtually undetectable by immunohistochemistry in cancerous tissues, compared to relatively high protein abundance in the normal mucosa (Figure 3C).

To validate that miR-25 exerts its biological activity through its effect on MCU, we transfected HeLa cells with short hairpin RNA (shRNA) targeting MCU: as for miR-25, shRNA-MCU decreases MCU abundance and increases proliferation (Figure S3A), indicating that MCU targeting is important for the growth-promoting activity of miR-25. We also tested the ability of MCU to inhibit the proliferation. We generated PC3 cells that stably expressed a MCU-FLAG-tagged construct (MCU-FLAG), in which MCU level and activity was increased relative to that in empty vector (pcDNA3) stable clones (Figures S3B and S3C), and found that they formed lower numbers of colonies in soft agar compared to control pcDNA3 stable clones (Figure S3D).

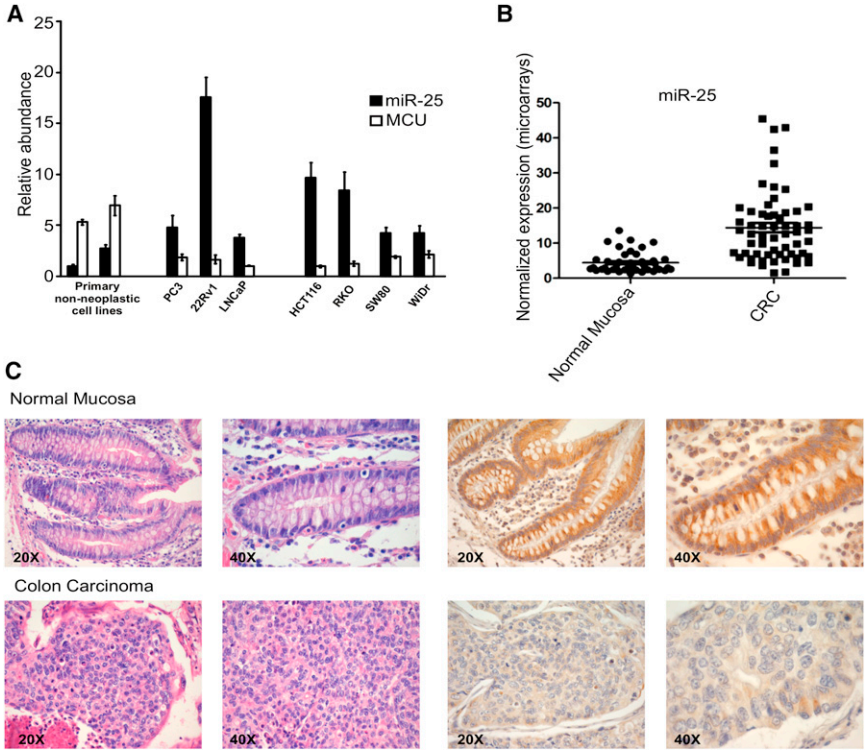

Figure 3. Inhibition of MCU Levels by miR-25 Is a Key Aspect in Human Colon Cancer Progression

(A) miR-25 and MCU mRNA expression levels were analyzed by quantitative real-time PCR in three prostate cancer (PC3, 22Rv1, LnCaP), four colon cancer (HCT116, RKO, SW80, WiDr), and primary nonneoplastic cell lines. RNU6B and 18S expression were used to normalize miR-25 and MCU expression results, respectively, for each sample. Primary nonneoplastic cells present very low abundance of miR-25 and high MCU levels, whereas cancer lines are characterized by inverse correlation between miR-25 levels and MCU mRNA expression. Error bars correspond to mean ± SEM of n = 3 independent experiments.

(B) miRNA expression was assessed in 44 normal mucosa samples and 59 stage 2–3 CRC samples via microarray. The graph shows the average expression level of miR-25 in both groups. miR-25 was significantly overexpressed in cancer samples, as compared to normal mucosa ($p < 0.0001$).

(C) Upper row: normal colonic mucosa (routinely stained with hematoxylin and eosin, at left) demonstrated strong cytoplasmic granular reactivity with the anti-MCU antibody (immunoperoxidase staining performed on formalin-fixed paraffin-embedded tissue sections, at right). Lower row: poorly differentiated colonic adenocarcinoma with solid pattern of growth (hematoxylin and eosin, at left) showing low level of reactivity with the anti-MCU antibody (immunoperoxidase staining, at right). Two neoplastic cells with cytoplasmic immunoreactivity of moderate intensity can be observed.

See also Figure S3.

We then investigated whether miR-25-dependent inhibition of mitochondrial Ca^{2+} uptake, and the ensuing resistance to apoptosis, could be specifically reversed in cancer cells. For this purpose, we overexpressed anti-miR-25 in the PC3 and HCT116 cells lines investigated in Figure 3. In both cell types, anti-miR-25 expression caused an ~40% increase in the $[Ca^{2+}]_m$ rise evoked by 100 μM ATP (Figures 4A and 4B). Accordingly, sensitivity to C2-ceramide and H_2O_2 were enhanced, as revealed by the lower viability (Figures 4C and 4D) and increased PARP and caspase-3 cleavage (Figures 4E and 4F) detected in anti-miR-25-expressing cells. These data were also confirmed measuring cellular positivity to annexin V (Figures S4A and S4B).

Overall, the data identify a microRNA (miR-25), highly expressed in cancer cells, that by targeting the newly discovered calcium channel of mitochondria reduces the sensitivity of cancer cells to apoptotic agents. This not only represents conclusive evidence of the key role of organelle Ca^{2+} accumulation in the mitochondria-dependent apoptotic routes but also highlights a novel, unexpected target in cancer therapy. Now, the exciting task of unveiling the structural and functional properties of this long-awaited component of the calcium signaling machinery of the cell finds an immediate translational application in a disease area of paramount importance.

Experimental Procedures

Cell Culture and Transient Transfection

HeLa, Hek293, HCT116, and RKO cells were cultured in Dulbecco's modified Eagle's medium supplemented with 10% fetal calf serum (FCS), L-glutamine, and penicillin/streptomycin in 75 cm^2 Falcon flasks. PC3, 22Rv1, and LnCaP cells were cultured in RPMI 1640, supplemented with 10% FCS, 2 mM L-glutamine, and penicillin/streptomycin, in 75 cm^2 Falcon flasks.

For aequorin experiments, cells were seeded onto 13 mm glass coverslips and allowed to grow to 75% confluence; for microscopy counts of cell viability, mitochondrial/reticular morphology analysis, and mitochondrial membrane potential measurements, cells were seeded on 24 mm glass coverslip in the same growth conditions.

Lipofectamine 2000 was used as transfectant according to the manufacturer's recommendations. For aequorin measurements, we used mtAEQmut for HeLa cells and mtAEQ for PC3 and HCT116 cells. All measurements were performed 24 hr after transfection. All miR and anti-miR molecules (hsa-miRNA precursor and hsa-miRNA inhibitor) were purchased from Ambion. shRNA targeting MCU (TRCN0000133861) was purchased from Sigma-Aldrich.

Vectors and Luciferase Assay

Portions of 3′ UTR of human MCU and MICU1 genes, containing miR-25 putative target regions, were amplified through PCR; primers are indicated in Supplemental Experimental Procedures.

Real-Time RT-PCR to Evaluate miRNA and mRNA Expression

Total RNA was extracted from cells with TRIzol reagent (Invitrogen) according to the manufacturer's instructions (see Supplemental Experimental Procedures).

Aequorin Measurements

Probes employed were chimeric aequorins targeted to the endoplasmic reticulum (erAEQmut), cytosol (cytAEQ), and mitochondria (mtAEQmut). "AEQ" refers to wild-type aequorin, and "AEQmut" refers to a low-affinity D119A mutant of aequorin, as described previously (see Supplemental Experimental Procedures and [15]).

Immunoblotting

Total cell lysates were prepared in RIPA buffer, and standard immunoblotting procedures were used (Supplemental Experimental Procedures).

Apoptosis Assay

After 24 hr transfection with the indicated miR, cells were treated with apoptotic stimuli (H_2O_2, C2-ceramide, or staurosporine), washed three

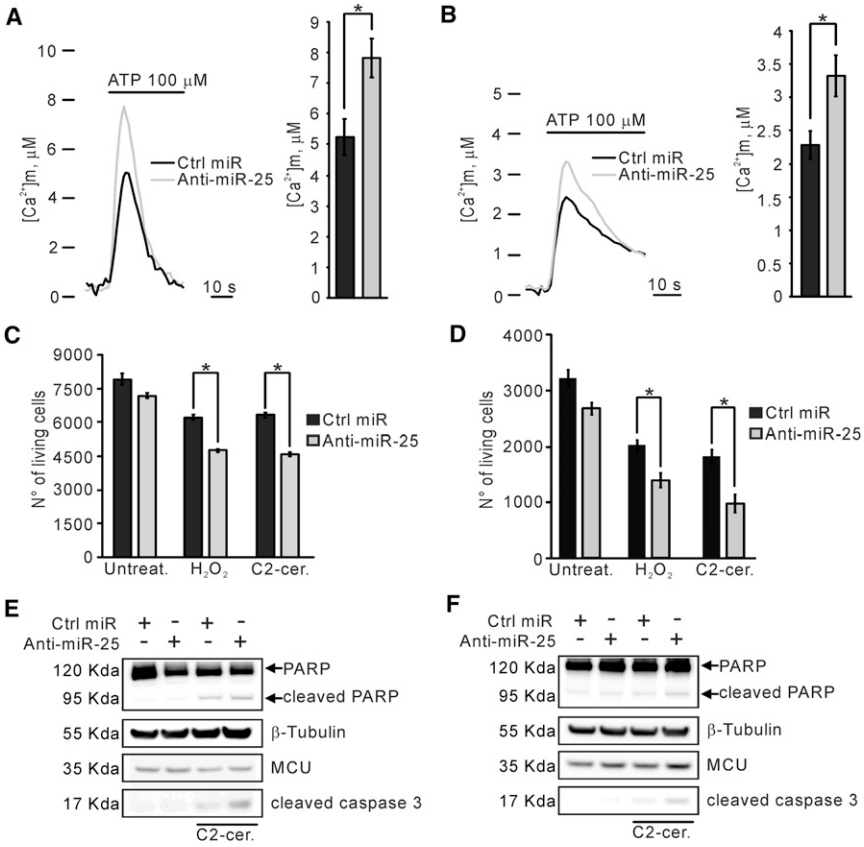

Figure 4. Regulation of miR-25 Levels Strongly Sensitizes Cells to Ca^{2+}-Dependent Apoptotic Stimuli

(A) $[Ca^{2+}]_m$ peaks in PC3 cells: Ctrl miR: 5.25 ± 0.59 μM; anti-miR-25: 7.81 ± 0.64 μM. n = 16 independent experiments.

(B) $[Ca^{2+}]_m$ peaks in HCT116 cells: Ctrl miR: 2.28 ± 0.21 μM; anti-miR-25: 3.32 ± 0.31 μM. n = 16 independent experiments.

(C and D) Microscopy counts of cell viability in PC3 (C) and HCT116 (D) cells. Treatments with H_2O_2 (500 μM for 2 hr) and C2-ceramide (C2-cer.; 40 μM for 2 hr) reveal a more efficient apoptosis induction after anti-miR-25 transfection. n = 3 independent experiments.

(E and F) Immunoblot shows increased levels of cleaved PARP and cleaved caspase-3 in anti-miR-25-expressing PC3 (E) and HCT116 (F) cells after treatment with C2-ceramide (C2-cer.; 40 μM for 2 hr).

*p < 0.05; error bars correspond to mean ± SEM. See also Figure S4.

times in PBS, and then fixed with 4% formaldehyde for 10 min at room temperature (RT). Cells were rinsed with PBS, and 0.1 μg/ml DAPI was added for 10 min at RT. After washing with PBS, the cells were detected with fluorescence microscopy, and cells with condensed and/or fragmented chromatin indicative of apoptosis were not counted as living cells. 250 fields per well were counted using a Scan^R high-content-throughput system (Olympus).

Immunohistochemistry

Sections (4 μm thick) were cut from formalin-fixed paraffin-embedded blocks. One section for each block was routinely stained with hematoxylin and eosin for histological examination (Supplemental Experimental Procedures).

Microarray and Data Analysis

RNA labeling and hybridization on microRNA microarray chips (ArrayExpress accession number A-MEXP-258) were performed as described previously [25]. Raw data were normalized and analyzed in GeneSpring GX software version 7.3 (Silicon Genetics or Agilent Technologies). Values below 0.01 were set to 0.01. Each measurement was divided by the 50th percentile of all measurements in that sample. GeneSpring software generated a unique value for each miRNA, performing the average of four probes. Graphs and statistical analyses were performed using GraphPad Prism 5 software.

Supplemental Information

Supplemental Information includes four figures, one table, and Supplemental Experimental Procedures and can be found with this article online at http://dx.doi.org/10.1016/j.cub.2012.11.026.

Acknowledgments

We thank E. Magri for technical assistance. This research was supported by the Italian Association for Cancer Research (AIRC); Telethon (GGP09128 and GGP11139B); local funds from the University of Ferrara; the Italian Ministry of Education, University and Research (COFIN, FIRB, and Futuro in Ricerca); the Italian Cystic Fibrosis Research Foundation and Italian Ministry of Health to P.P.; the Italian Ministry of Health to A.R.; grants from the Italian Ministry of Health and Ministry of Education, University and Research, the European Union (ERC mitoCalcium, 294777 and FP7 "MyoAGE," 223576), the National Institutes of Health (#1P01AG025532-01A1), the Cariparo Foundation (Padua), AIRC, and Telethon-Italy (GPP1005A, GGP11082) to R.R.; and grants from AIRC, the Italian Ministry of Education, University and Research, FIRB program 2011 (RBAP11BYNP), and Regione Emilia Romagna to M.N. S. Marchi was supported by a FIRC fellowship.

Received: August 16, 2012
Revised: October 22, 2012
Accepted: November 12, 2012
Published: December 13, 2012

References

1. Baughman, J.M., Perocchi, F., Girgis, H.S., Plovanich, M., Belcher-Timme, C.A., Sancak, Y., Bao, X.R., Strittmatter, L., Goldberger, O., Bogorad, R.L., et al. (2011). Integrative genomics identifies MCU as an essential component of the mitochondrial calcium uniporter. Nature *476*, 341–345.
2. De Stefani, D., Raffaello, A., Teardo, E., Szabò, I., and Rizzuto, R. (2011). A forty-kilodalton protein of the inner membrane is the mitochondrial calcium uniporter. Nature *476*, 336–340.
3. Clapham, D.E. (2007). Calcium signaling. Cell *131*, 1047–1058.
4. Pinton, P., Giorgi, C., Siviero, R., Zecchini, E., and Rizzuto, R. (2008). Calcium and apoptosis: ER-mitochondria Ca2+ transfer in the control of apoptosis. Oncogene *27*, 6407–6418.
5. Giorgi, C., Baldassari, F., Bononi, A., Bonora, M., De Marchi, E., Marchi, S., Missiroli, S., Patergnani, S., Rimessi, A., Suski, J.M., et al. (2012). Mitochondrial Ca(2+) and apoptosis. Cell Calcium *52*, 36–43.
6. Roderick, H.L., and Cook, S.J. (2008). Ca2+ signalling checkpoints in cancer: remodelling Ca2+ for cancer cell proliferation and survival. Nat. Rev. Cancer *8*, 361–375.

7. Perocchi, F., Gohil, V.M., Girgis, H.S., Bao, X.R., McCombs, J.E., Palmer, A.E., and Mootha, V.K. (2010). MICU1 encodes a mitochondrial EF hand protein required for Ca(2+) uptake. Nature *467*, 291–296.
8. Filipowicz, W., Bhattacharyya, S.N., and Sonenberg, N. (2008). Mechanisms of post-transcriptional regulation by microRNAs: are the answers in sight? Nat. Rev. Genet. *9*, 102–114.
9. Bartel, D.P. (2009). MicroRNAs: target recognition and regulatory functions. Cell *136*, 215–233.
10. Lovat, F., Valeri, N., and Croce, C.M. (2011). MicroRNAs in the pathogenesis of cancer. Semin. Oncol. *38*, 724–733.
11. Lewis, B.P., Burge, C.B., and Bartel, D.P. (2005). Conserved seed pairing, often flanked by adenosines, indicates that thousands of human genes are microRNA targets. Cell *120*, 15–20.
12. Maragkakis, M., Reczko, M., Simossis, V.A., Alexiou, P., Papadopoulos, G.L., Dalamagas, T., Giannopoulos, G., Goumas, G., Koukis, E., Kourtis, K., et al. (2009). DIANA-microT web server: elucidating microRNA functions through target prediction. Nucleic Acids Res. *37* (Web Server issue), W273–W276.
13. Dong, H., Paquette, M., Williams, A., Zoeller, R.T., Wade, M., and Yauk, C. (2010). Thyroid hormone may regulate mRNA abundance in liver by acting on microRNAs. PLoS ONE *5*, e12136.
14. John, B., Enright, A.J., Aravin, A., Tuschl, T., Sander, C., and Marks, D.S. (2004). Human MicroRNA targets. PLoS Biol. *2*, e363.
15. Pinton, P., Rimessi, A., Romagnoli, A., Prandini, A., and Rizzuto, R. (2007). Biosensors for the detection of calcium and pH. Methods Cell Biol. *80*, 297–325.
16. Scorrano, L., Oakes, S.A., Opferman, J.T., Cheng, E.H., Sorcinelli, M.D., Pozzan, T., and Korsmeyer, S.J. (2003). BAX and BAK regulation of endoplasmic reticulum Ca2+: a control point for apoptosis. Science *300*, 135–139.
17. Pinton, P., Ferrari, D., Rapizzi, E., Di Virgilio, F., Pozzan, T., and Rizzuto, R. (2001). The Ca2+ concentration of the endoplasmic reticulum is a key determinant of ceramide-induced apoptosis: significance for the molecular mechanism of Bcl-2 action. EMBO J. *20*, 2690–2701.
18. Garrido, C., Galluzzi, L., Brunet, M., Puig, P.E., Didelot, C., and Kroemer, G. (2006). Mechanisms of cytochrome c release from mitochondria. Cell Death Differ. *13*, 1423–1433.
19. Giorgi, C., De Stefani, D., Bononi, A., Rizzuto, R., and Pinton, P. (2009). Structural and functional link between the mitochondrial network and the endoplasmic reticulum. Int. J. Biochem. Cell Biol. *41*, 1817–1827.
20. Grimm, S. (2012). The ER-mitochondria interface: the social network of cell death. Biochim. Biophys. Acta *1823*, 327–334.
21. Simmen, T., Lynes, E.M., Gesson, K., and Thomas, G. (2010). Oxidative protein folding in the endoplasmic reticulum: tight links to the mitochondria-associated membrane (MAM). Biochim. Biophys. Acta *1798*, 1465–1473.
22. Zhang, H., Zuo, Z., Lu, X., Wang, L., Wang, H., and Zhu, Z. (2012). MiR-25 regulates apoptosis by targeting Bim in human ovarian cancer. Oncol. Rep. *27*, 594–598.
23. Razumilava, N., Bronk, S.F., Smoot, R.L., Fingas, C.D., Werneburg, N.W., Roberts, L.R., and Mott, J.L. (2012). miR-25 targets TNF-related apoptosis inducing ligand (TRAIL) death receptor-4 and promotes apoptosis resistance in cholangiocarcinoma. Hepatology *55*, 465–475.
24. Poliseno, L., Salmena, L., Riccardi, L., Fornari, A., Song, M.S., Hobbs, R.M., Sportoletti, P., Varmeh, S., Egia, A., Fedele, G., et al. (2010). Identification of the miR-106b~25 microRNA cluster as a proto-oncogenic PTEN-targeting intron that cooperates with its host gene MCM7 in transformation. Sci. Signal. *3*, ra29.
25. Lanza, G., Ferracin, M., Gafà, R., Veronese, A., Spizzo, R., Pichiorri, F., Liu, C.G., Calin, G.A., Croce, C.M., and Negrini, M. (2007). mRNA/microRNA gene expression profile in microsatellite unstable colorectal cancer. Mol. Cancer *6*, 54.
26. Nishida, N., Nagahara, M., Sato, T., Mimori, K., Sudo, T., Tanaka, F., Shibata, K., Ishii, H., Sugihara, K., Doki, Y., and Mori, M. (2012). Microarray analysis of colorectal cancer stromal tissue reveals upregulation of two oncogenic miRNA clusters. Clin. Cancer Res. *18*, 3054–3070.

Current Biology, Volume *23*

Supplemental Information

Downregulation of the Mitochondrial Calcium Uniporter by Cancer-Related miR-25

Saverio Marchi, Laura Lupini, Simone Patergnani, Alessandro Rimessi, Sonia Missiroli, Massimo Bonora, Angela Bononi, Fabio Corrà, Carlotta Giorgi, Elena De Marchi, Federica Poletti, Roberta Gafà, Giovanni Lanza, Massimo Negrini, Rosario Rizzuto, and Paolo Pinton

Author Contributions

S. Marchi conceived and performed all experiments, collected and analyzed experimental data, and prepared the manuscript. S.P., A.R., S. Missiroli, A.B., E.D.M., F.P. and C.G. assisted with cell culture and performed some experiments. M.B. assisted with imaging-based experiments. L.L. and F.C. performed quantitative RT-PCR experiments. R.G. and G.L. performed immunohistochemistry experiments and reviewed all experimental data. R.R. and M.N. reviewed all experimental data, and prepared the manuscript. P.P. conceived all experiments, reviewed all experimental data, and prepared the manuscript. All authors discussed the results and reviewed the manuscript.

Supplemental Inventory

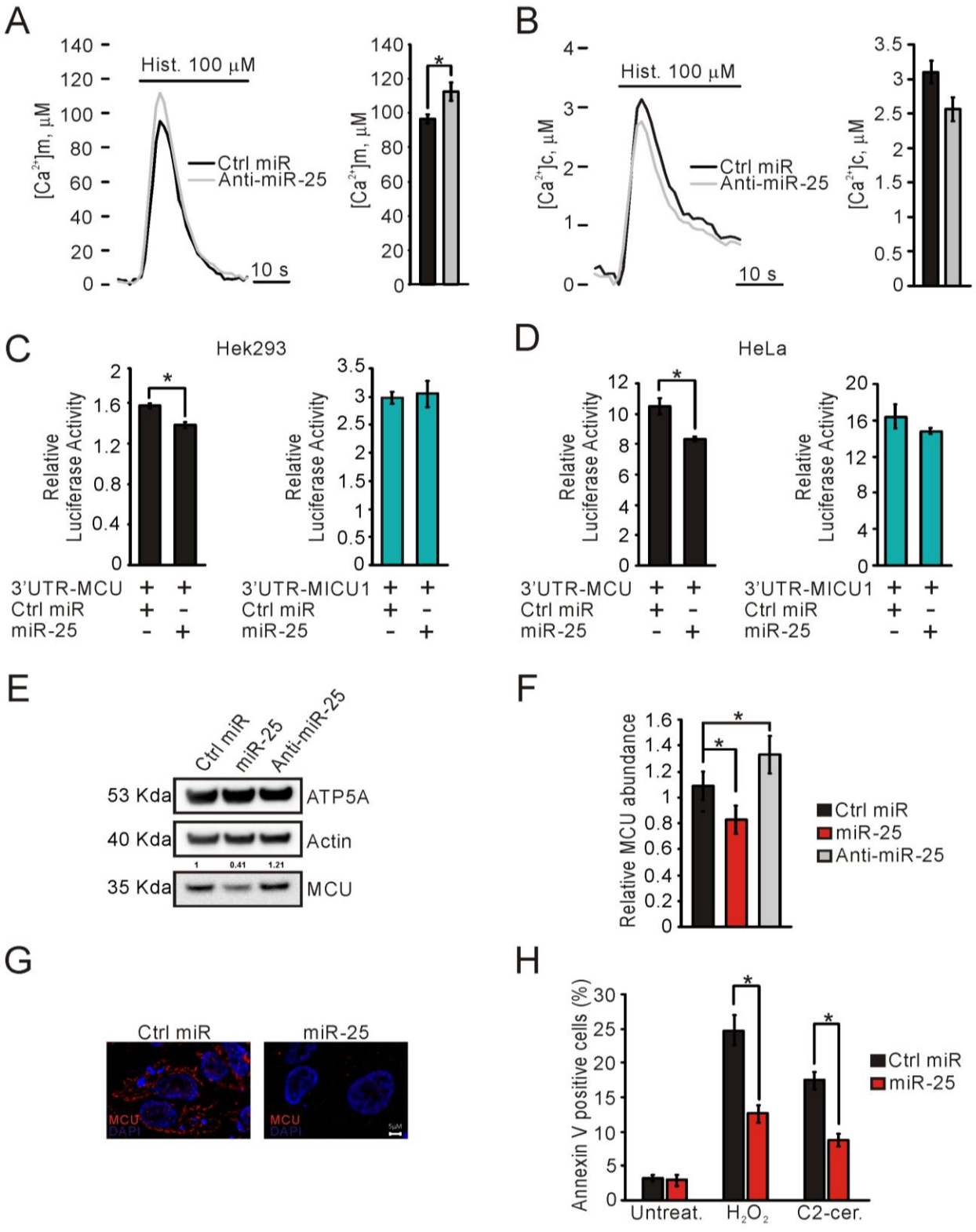
A
Hist. 100 μM
Ctrl miR
Anti-miR-25
10 s
[Ca2+]m, μM
B
Hist. 100 μM
Ctrl miR
Anti-miR-25
10 s
[Ca2+]c, μM
C
Hek293
Relative Luciferase Activity
3'UTR-MCU
3'UTR-MICU1
Ctrl miR
miR-25
D
HeLa
E
Ctrl miR
miR-25
Anti-miR-25
53 Kda
ATP5A
40 Kda
Actin
35 Kda
MCU
F
Relative MCU abundance
Ctrl miR
miR-25
Anti-miR-25
G
Ctrl miR
miR-25
MCU
DAPI
H
Annexin V positive cells (%)
Ctrl miR
miR-25
Untreat.
H2O2
C2-cer.

Figure S1.

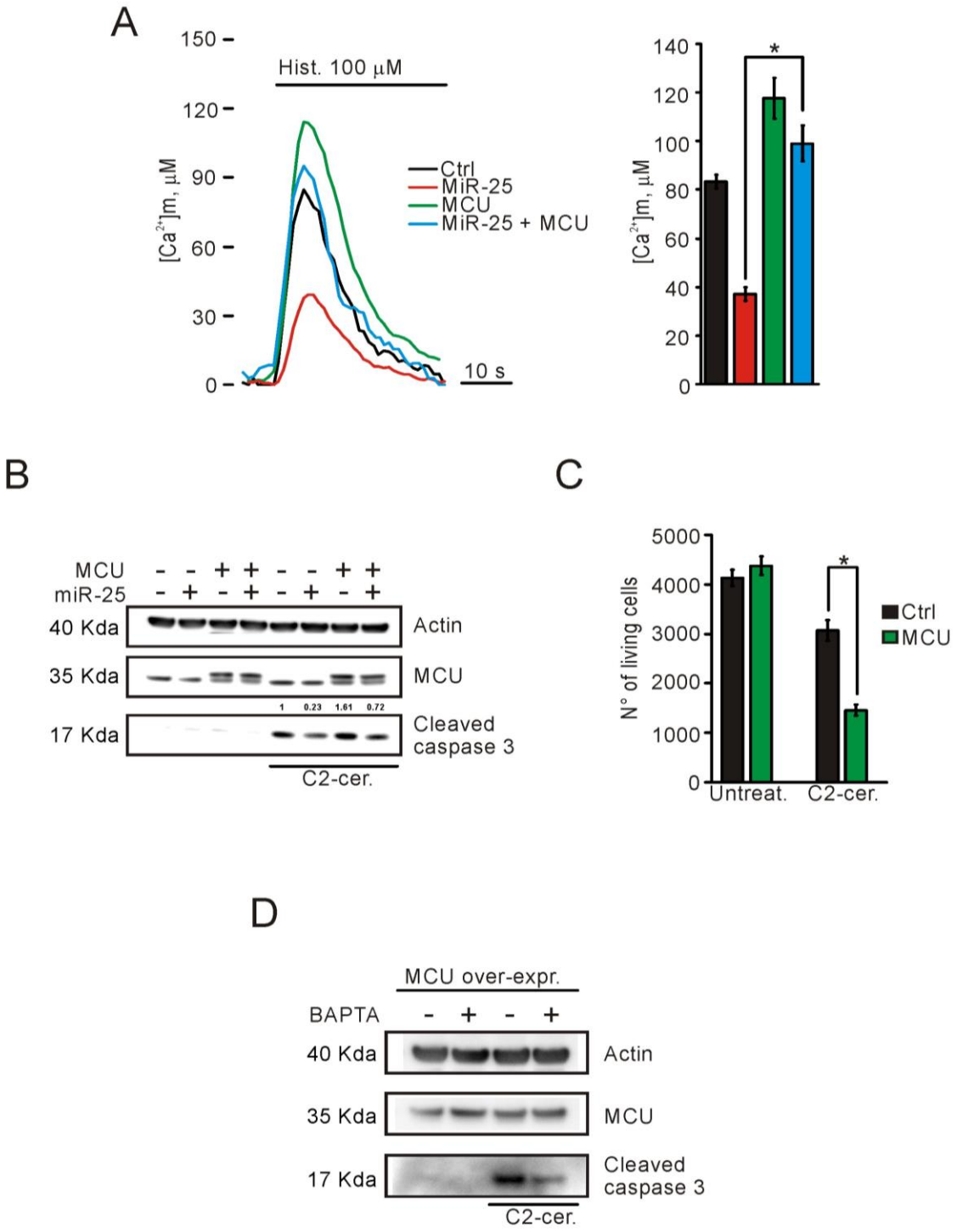
A
Hist. 100 µM
[Ca2+]m, µM
Ctrl
MiR-25
MCU
MiR-25 + MCU
10 s
*
B
MCU
miR-25
40 Kda
Actin
35 Kda
MCU
17 Kda
Cleaved caspase 3
1
0.23
1.61
0.72
C2-cer.
C
N° of living cells
Ctrl
MCU
Untreat.
C2-cer.
D
MCU over-expr.
BAPTA
40 Kda
Actin
35 Kda
MCU
17 Kda
Cleaved caspase 3
C2-cer.

Figure S2.

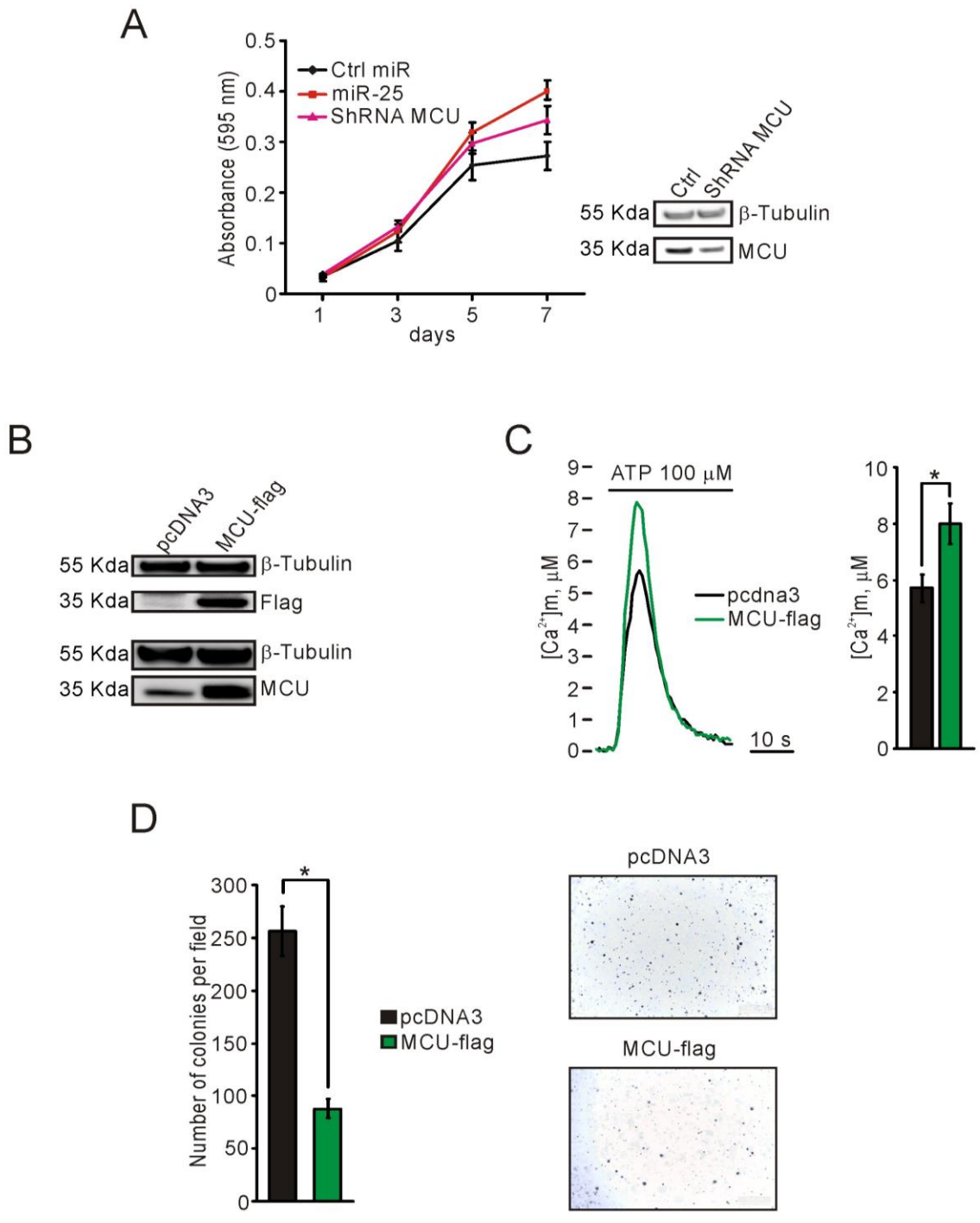
A
Absorbance (595 nm)
0.5
0.4
0.3
0.2
0.1
0
Ctrl miR
miR-25
ShRNA MCU
1
3
5
7
days
Ctrl
ShRNA MCU
55 Kda
β-Tubulin
35 Kda
MCU
B
pcDNA3
MCU-flag
55 Kda
β-Tubulin
35 Kda
Flag
55 Kda
β-Tubulin
35 Kda
MCU
C
ATP 100 μM
[Ca2+]m, μM
pcdna3
MCU-flag
10 s
*
D
Number of colonies per field
300
250
200
150
100
50
0
*
pcDNA3
MCU-flag
pcDNA3
MCU-flag

Figure S3.

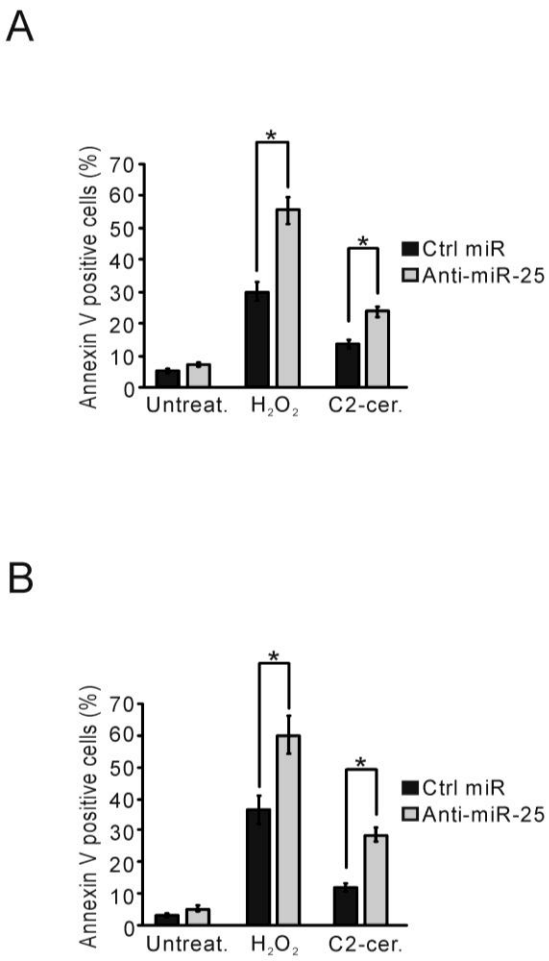

Figure S4.

Table S1.

		miRNA prediction						
miRNA	Target	Tot.	Targetscan	microT	microCosm	Miranda	Cancer Link	
miR-15/16/195/424/497	MCU/MICU1	2/4	X X	X X	X	X	Yes	Down
miR-17-5p/20/93.mr/106/519.d	MCU	1	X				Yes	Up
miR-21/590-5p	MCU	3	X		X	X	Yes	Up
miR-25/32/92/92ab/363/367	MCU/MICU1	3/3	X X	X	X	X X	Yes	Up
miR-137	MCU	4	X	X	X	X	Yes	Down

Table 1 lists some microRNAs involved in human cancer, which target MCU and MICU1 messengers RNA. For each group are indicated which algorithms (Targetscan, microT, microCosm, Miranda) were able to predict the targeting and if these microRNAs were found up or downregulated in human cancer.

Supplemental Figure Legends

Figure S1. Anti-miR-25 Expression Increases MCU Levels and Mitochondrial Ca^{2+} Uptake in HeLa Cells, Related to Figure 1

(**A**) Where indicated mitochondrially targeted aequorin (mtAEQmut)–transfected cells were treated with 100 μM Histamine (Hist.). Mitochondrial Ca^{2+} concentration ($[Ca^{2+}]_m$) peaks: Negative Control (Ctrl mir): 96.63 ± 2.71 μM; Anti-miR-25: 112.58 ± 5.41 μM.

(**B**) Cytosolic Ca^{2+} concentration peaks: Ctrl miR: 3.10 ± 0.167 μM; Anti-miR-25: 2.56 ± 0.172 μM.

(**C-D**) Luciferase assays were performed in Hek293 and HeLa cells. psiCHECK-3'UTR-MCU or psiCHECK-3'UTR-MICU1 constructs were co-transfected with miR-25 or Ctrl miR. Renilla luciferase activity was normalized on firefly luciferase activity. Relative luciferase activity of psiCHECK-3'UTR-MCU displayed 12% and 20% decrease following miR-25 enforced expression if compared to negative control, respectively in Hek293 (**C**) and HeLa (**D**) cells. No significant differences were found in relative luciferase activity of psiCHECK-3'UTR-MICU1 construct in both cell lines.

(**E**) Immunoblot analysis of MCU protein after miR-25 and anti-miR-25 expression in HeLa cells. ATP5A has been used as inner mitochondrial membrane marker. Quantification of MCU protein is reported.

(**F**) MCU mRNA expression was assessed through quantitative Real Time PCR in HeLa cells transfected with miR-25, anti-miR-25 or Ctrl miR. GAPDH expression was used to normalize MCU expression results for each sample. MiR-25 enforced expression caused a 30% decrease in MCU mRNA levels, whereas anti-miR-25 transfection induced a 28% increase in MCU expression, if compared to control transfected cells.

(**G**) Immunofluorescence showing MCU down-regulation by miR-25.

(**H**) HeLa cells were treated with Hydrogen Peroxide (H_2O_2; 500 μM for 2 h.) or C2-ceramide (C2-cer.; 40 μM for 2 h.), and subsequently stained with annexin V-Alexa fluor 488.

Error bars correspond to mean ± SEM of at least three independent experiments. *$p < 0.05$.

Figure S2. MCU Reintroduction Restores miR-25 Activity, Related to Figure 2

(**A**) Mitochondrial Ca^{2+} concentration ($[Ca^{2+}]_m$) peaks: Negative Control (Ctrl miR): 83.36 ± 2.656 μM; mir-25: 39.04 ± 2.875 μM; MCU: 118.63 ± 8.5 μM; mir-25 + MCU: 99.06 ± 7.4 μM.

(**B**) Immunoblot analysis showing cleaved caspase 3 levels, after treatment with C2-cer (40 μM for 2 h.). Quantification of cleaved caspase 3 protein is reported.

(**C**) Microscopy counts of cell viability after treatment with C2-ceramide (40 μM for 2 h.), in 22Rv1 cells, after MCU over-expression.

(**D**) Immunoblot analysis of MCU-overexpressing HeLa cells, showing cleaved caspase 3 levels, after treatment with C2-cer (40 μM for 2 h.). Where indicated, cells were pre-treated (5 μM, 20 min) with the intracellular Ca^{2+} buffer BAPTA-AM (Invitrogen).

Error bars correspond to mean ± SEM of at least three independent experiments. *$p < 0.05$.

Figure S3. miR-25 Proto-oncogenic Activity, Related to Figure 3

(**A**) Growth curve of HeLa cells after miR-25 or ShRNA MCU expression. Immunoblot analysis on the right.

(**B**) Immunoblot analysis of PC3 cells stably expressing pcDNA3 empty vector (pcDNA3) or MCU-flag tagged, in pcDNA3 vector (MCU-flag).

(**C**) Mitochondrial Ca^{2+} concentration ($[Ca^{2+}]_m$) peaks: pcDNA3: 5.7 ± 0.47 μM; MCU-flag: 8 ± 0.71 μM.

(**D**) Number of colonies formed in soft agar; representative fields on the right.

Error bars correspond to mean ± SEM of at least three independent experiments. *$p < 0.05$.

Figure S4. Anti-miR-25 Sensitizes PC3 and HCT116 Cells to Apoptosis, Related to Figure 4

PC3 (**A**) and HCT116 (**B**) cells were treated with Hydrogen Peroxide (H_2O_2; 500 μM for 2 h.) or C2-ceramide (C2-cer.; 40 μM for 2 h.), and subsequently stained with annexin V-Alexa fluor 488. Percentage of Annexin V-positive cells is shown. Error bars correspond to mean ± SEM of three independent experiments. *$p < 0.05$.

Supplemental Experimental Procedures

Vectors and Luciferase Assay

Portions of 3'UTR of human MCU and MICU1 genes, containing miR-25 putative target regions, were amplified through PCR, using the following primers:
MCU_3UTR_F: 5'-CACTCGAGACACTGCATGAGGTTGTTGG-3'
MCU_3UTR_R: 5'-CAGTTTAAACCACCTGGAGTCTGGGTTTGT-3' (760 bp);
MICU1_3UTR_F: 5'-CACTCGAGAGAATTCAGGGAACCATCCA-3'
MICU1_3UTR_R: 5'-CAGTTTAAACACAGGGAACTTTGGGGATGT-3' (570 bp).
These regions were cloned into psiCHECK-2 vector (Promega), downstream of renilla luciferase gene, using XhoI and PmeI restriction sites. For luciferase assay Hek-293 and Hela cells were cultured in 24-well plate and transfected in triplicate with 400 ng of psiCHECK-3'UTR-MCU, psiCHECK-3'UTR-MICU1 constructs or psiCHECK control vector and 50 pmol of miR-25 or Negative Control 2 (Ambion). Transfection was performed using Lipofectamine 2000 and Optimem I Reduced Serum Medium (Invitrogen), as described by the manufacturer. Luciferase activity measurement was performed 24 hours after transfection, using Dual-Luciferase Reporter Assay (Promega), following the protocol of the kit. Activity of firefly luciferase was used to normalize renilla luciferase activity, for each well.

Real-Time RT-PCR to Evaluate miRNA and mRNA Expression

Total RNA was extracted from cells with Trizol reagent (Invitrogen), according to the manufacturer's instructions. Mature miR-25 expression was assessed using TaqMan microRNA assay – has-miR-25-3p (Applied Biosystem – 000403) and normalized on RNU6B (Applied Biosystem – 001093). Five ng of total RNA were reverse-transcribed using TaqMan MicroRNA Reverse Transcription kit (Applied Biosystem) and the looped primer provided by the specific TaqMan microRNA assay. The quantitative PCR reaction mix was prepared using TaqMan Universal PCR Master Mix, No Amperase UNG (Applied Biosystem) and specific TaqMan primers and probe provided by TaqMan microRNA assay kits. Reactions were carried out in a 96-well plate at 95°C for 10 min, followed by 40 cycles of 95°C for 15 sec and 60°C for 1 min, on Bio-Rad-Chromo4 Real Time thermal Cycler. Each sample was analyzed in triplicate. The level of miRNA was measured using Ct (threshold cycle) and to calculate the amount of miRNA, the method of 2-ΔΔCt was used. To analyze mRNA expression, qRT-PCR was performed on 500 ng of total RNA using oligo dT (Fermentas) and random primers (Gibco). Quantitative PCR reaction was performed using Qiagen Taq DNA Polymerase (Qiagen) and EvaGreen (Biotium Inc). The following oligonucleotides were used as primers for the qPCR reaction:
MCU_RT_F: 5'-TTCCTGGCAGAATTTGGGAG-3'
MCU_RT_R: 5'- AGAGATAGGCTTGAGTGTGAAC-3'
GAPDH_RT_F: 5'-CTATAAATTGAGCCCGCAGCC-3'
GAPDH_RT_R: 5'-CCCAATACGACCAAATCCGT-3'
18S_RT_F: 5'- CTGCCCTATCAACTTTCGATGGTAG-3'
18S_RT_R: 5'-CCGTTTCTCAGGCTCCCTCTC-3'.
Reactions were incubated in a 96-well PCR plate at 95°C for 15 min, followed by 40 cycles of 95° C for 30 sec and 58°C for 1 min, on Bio-Rad-Chromo4 Real Time thermal Cycler. Each sample was analyzed in triplicate. 18S RNA expressions were used as endogenous reference control. The level of mRNA was measured using Ct (threshold cycle) and to calculate the amount of mRNA, the method of 2-ΔΔCt was used.

Aequorin Measurements

Probes employed are chimeric aequorins targeted to the endoplasmic reticulum (erAEQmut), cytosol (cytAEQ), and mitochondria (mtAEQmut). "AEQ" refers to wild-type aequorin, and "AEQmut" refers to a low affinity D119A mutant of aequorin. For the experiments with cytAEQ, mtAEQ and mtAEQmut, cells were incubated with 5 μM coelenterazine for 1–2 h in Dulbecco's modified Eagle's medium supplemented with 1% fetal calf serum. A coverslip with transfected cells was placed in a perfused thermostated chamber located in close proximity to a low noise photomultiplier with a built-in amplifier/discriminator. To reconstitute erAEQmut with high efficiency, the luminal [Ca^{2+}] of the ER first had to be reduced. This was achieved by incubating cells for 1 h at 4°C in Krebs-Ringer buffer (KRB) supplemented with 5 μM coelenterazine, 5 μM Ca^{2+} ionophore ionomycin (Sigma-Aldrich), and 600 μM EGTA. After this incubation, cells were extensively washed with KRB supplemented with 2% bovine serum albumin and then transferred to the perfusion chamber. All aequorin measurements were carried out in KRB supplemented with either 1 mM $CaCl_2$ (cytAEQ and mtAEQmut) or 100 μM EGTA (erAEQmut). Agonist was added to the same medium as specified in figure legends. The experiments were terminated by lysing cells with 100 μM digitonin in a hypotonic Ca^{2+}-containing solution (10 mM $CaCl_2$ in H_2O), thus discharging the remaining aequorin pool. The output of the discriminator was captured by a Thorn EMI photon-counting board and stored in an IBM-compatible computer for further analyses. The aequorin luminescence data were calibrated offline into [Ca^{2+}] values using a computer algorithm based on the Ca^{2+} response curve of wild-type and mutant aequorins.

In the experiments with permeabilized cells, a buffer mimicking the cytosolic ionic composition, (intracellular buffer) was used: 130 mM KCl, 10 mM NaCl, 2 mM K_2HPO_4, 5 mM succinic acid, 5 mM malic acid, 1 mM $MgCl_2$, 20 mM HEPES, 1 mM pyruvate, 0.5 mM ATP and 0.1 mM ADP (pH 7 at 37 °C). Intracellular buffer was supplemented with either 100 μM EGTA (intracellular buffer/EGTA) or a 2 mM EGTA and 2 mM HEEDTA-buffered [Ca^{2+}] of 1 or 4 μM (intracellular buffer/Ca^{2+}), calculated with the Chelator software [27]. HeLa cells were permeabilized by a 1-min perfusion with 50 μM digitonin (added to intracellular buffer/EGTA) during luminescence measurements. Mitochondrial Ca^{2+} uptake rate was calculated as the first derivative by using the OriginLab® software. The higher value reached during Ca^{2+} addition represents the maximal Ca^{2+} uptake rate.

Mitochondrial Membrane Potential (ΔΨm) Measurements

HeLa cells were seeded and transfected with the indicated miR. MiR expression was allowed for 24 hours and mitochondrial ΔΨ was measured by loading cells with 20 nM tetramethyl rhodamine methyl ester (TMRM, Invitrogen) for 30 min at 37 °C. Successively, cells where imaged with Nikon Swept Field Confocal equipped with CFI Plan Apo VC60XH objective (n.a. 1.4) and an Andor DU885 EM-CCD camera, controlled by the NIS-Elements 3.2. Basal levels were normalized on fluorescence in presence of FCCP (carbonyl cyanide p-trifluoromethoxyphenylhydrazone, 10 μM), a strong uncoupler of oxidative phosphorylation.

Imaging and Analysis of Mitochondrial Morphology

HeLa cells were seeded on 24-mm coverslips and transfected using Lipofectamine 2000 as previously described. During transfection control miR or miR-25 were cotransfected with mt-DsRed and ErGFP.

At 24 hours after transfection, cells were imaged with a laser scanning confocal Zeiss LSM 510, illuminating GFP at 488 nm and dsRed at 543 nm. Z stack of 51 planes were obtained with an objective Plan-Apo 63x/1.4 Oil Ph3 with a voxel size of 105 x 105 x 200 nm (X x Y x Z). To obtain the best object reality, images were next deconvolved using the open source software Fiji (http://fiji.sc/wiki/index.php/Fiji, last accessed June 20, 2011), and especially through the 3D iterative deconvolution plugin (http://www.optinav.com/Iterative-Deconvolve-3D.htm). A theoretical PSF were build using the "PSF generator" plugin available at http://bigwww.epfl.ch/algorithms/psfgenerator/.

Once reconstructed a mitochondrial and endoplasmic reticulum mask were manually chosen to obtain a binarized image of overlapping areas. The resulting areas were described in number and volume, using the 3D object counter, available in Fiji.

Immunoblotting

Total cell lysates were prepared in RIPA buffer and the standard immunoblotting procedure was used. Proteins were quantified by the bicinchoninic acid assay (BCA) method and 20 μg of each sample were loaded on a Novex NuPage Bis-Tris 4–12% precast gel (Invitrogen) and transferred onto nitrocellulose membranes. Isotype-matched, horseradish-peroxidase-conjugated secondary antibodies (Santa Cruz Biotech.) were used, followed by detection by chemiluminescence (ThermoScientific), using ImageQuant LAS 4000 (GE Healthcare).

Primary antibodies used were: rabbit anti-PARP and rabbit anti-Caspase 3 from Cell Signalling; rabbit anti-Actin, rabbit anti-MCU, rabbit anti-Flag and mouse anti-β tubulin from Sigma-Aldrich; rabbit anti-MICU1 and rabbit anti-ATP5A from Abcam.

Immunohistochemistry

Four-micrometer thick sections were cut from formalin-fixed paraffin-embedded blocks. One section for each block was routinely stained with hematoxylin and eosin for histological examination.

For immunodetection of MCU, tissue sections were deparaffinized with xilene and rehydrated by sequential ethanol (from 100% to 80%) and rinsed in distilled water. Before immunostaining, sections were processed by microwave-oven for antigen retrival in Tris-EDTA-Citrate buffer (pH 7.8) for 30 minutes. After rinse with distilled water and rehydratation with PBS buffer, sections were incubated in a buffer solution with 3% of H_2O_2 for 15 minutes at room temperature to block endogenous peroxidase activity.

Tissue sections were then incubated with the primary rabbit anti-MCU antibody (Sigma-Aldrich), diluted 1:100 for 1h at room temperature. We then used the Ultravision Detection System (Large Volume Polyvalent-HRP) (Thermo Scientific) and the Dab Detection Kit (Cell Marque) according to manufacturers' instructions. Counterstaining was conducted with Mayer's hematoxylin.

Immunofluorescence

Cells were fixed with 4% formaldehyde for 10 min at RT. After washing three times with phosphate-buffered saline (PBS), cells were permeabilized with 0.1% Triton X-100 in PBS (PBST) at RT for 10 min and treated with PBST containing 5% skim milk (PBSTM) at RT for 1 h. Cells were incubated with antibody to MCU in PBSTM overnight at 4 °C, washed three times with PBS, and then incubated with Alexa-594-conjugated anti-rabbit IgG (Molecular Probes) at RT for 1 h.

Images were acquired through an epifluorescent microscope Axiovert 200M (ZEISS) equipped with a 100x Pla-Neofluar n.a. 1.3 (Zeiss) and a CoolSnap HQ (Photometrics). Each field was acquired as z-stack (21 planes spaced by 0.5 μM) then deconvolved through the open source software Fiji (available at http://fiji.sc/) and the parallel iterative deconvolution plugin.

Cell Proliferation

8 hours after transfection, the cells of one 6-well dish were trypsinized, counted with Burker chamber, and plated in four sets of five wells of a 12-well plate. Starting from the following day (day 1), 1 set of wells (at days 3, 5 and 7) was washed once with PBS, fixed in 4% formaldehyde solution for 10 min at room temperature, and then kept in PBS at 4°C. At day 7, all the wells were stained with crystal violet. After lysis with 10% acetic acid, the absorbance was read at 595 nm.

Growth in Semisolid Medium

The bottom layer was obtained by covering six-well dishes with 3 ml of 0.6% agar in RPMI. The following day, 5×10^4 stable clone PC3 cells were plated on this bottom layer in triplicate, in 2 ml of 0.3% agar in RPMI + 10% FBS. After 4 weeks, colonies were stained with 0.005% crystal violet and counted at 4x magnification. Five fields for each well were counted. A Leica DM IL LED microscope was used. Colonies were counted automatically using a custom made macro in the Fiji software. Briefly, dark objects were thresholded using the Yen algorithm and counted through the analyze particles tool; objects smaller than 70 pixels were excluded.

Measurement of Annexin V Binding

Cells were centrifuged, washed with PBS and the cell pellet was resuspended in 100 μl of labelling solution, containing 5 μl annexin V Alexa fluor 488 reagent (Invitrogen). After 20 min incubation, according to manufacturer's instructions, cells were measured at Tali™ image-based cytometer (Invitrogen). Percentage of positive cells has been reported.

Statistical Analysis

In each graph, unless noted, data represent mean ± SEM. If indicated, statistical significance has been calculated by a two-tailed Student t-test between the indicated samples. p values are indicated in the legends.

Supplemental References

27. Schoenmakers, T.J., Visser, G.J., Flik, G., and Theuvenet, A.P. (1992). CHELATOR: an improved method for computing metal ion concentrations in physiological solutions. BioTechniques *12*, 870-874, 876-879.